Annealing effects on the structure and magnetic properties of Fe–C granular films

2004 J. Phys.: Condens. Matter 16 5569

(http://iopscience.iop.org/0953-8984/16/30/017)

INSTITUTE OF PHYSICS PUBLISHING JOURNAL OF PHYSICS: CONDENSED MATTER

J. Phys.: Condens. Matter **16** (2004) 5569–5582 PII: S0953-8984(04)77446-9

Annealing effects on the structure and magnetic properties of Fe–C granular films

W B Mi[1], Z Q Li[1], P Wu[1], E Y Jiang[1] and H L Bai[1,2,3]

[1] Tianjin Key Laboratory of Low Dimensional Materials Physics and Preparing Technology, Institute of Advanced Materials Physics, Faculty of Science, Tianjin University, Tianjin 300072, People's Republic of China

[2] Key Laboratory for Advanced Ceramics and Machining Technology of Ministry of Education, Tianjin University, Tianjin 300072, People's Republic of China

E-mail: baihaili@tju.edu.cn and baihaili@public.tpt.tj.cn

Received 8 March 2004, in final form 8 June 2004
Published 16 July 2004
Online at stacks.iop.org/JPhysCM/16/5569
doi:10.1088/0953-8984/16/30/017

Abstract

Fe–C granular films with different Fe volume fraction x_v were fabricated using a DC facing-target sputtering system at room temperature and subsequently annealed at different temperatures. X-ray diffraction and selected area electron diffraction analyses indicate that as-deposited and low-temperature annealed ($\leqslant$350 °C) samples are composed of amorphous Fe and C, and higher temperature annealing makes the amorphous Fe transform to α-Fe, which is also confirmed by high-resolution transmission electron microscopy. Magnetic measurements indicate that at room temperature the as-deposited Fe–C ($x_v = 58$) granular films are superparamagnetic and annealed ones are ferromagnetic. The coercivity of 100 nm thick Fe–C ($x_v = 58$) granular films increases with annealing temperature (for 1 h) and time (at 450 °C). The coercivity of the 100 nm thick Fe–C ($x_v = 58$) samples annealed at temperatures ranging from 400 to 500 °C decreases linearly with measuring temperature T, signalling a domain wall motion mechanism. For the samples annealed at 550 °C, the change of in-plane coercivity with T satisfies the relation $H_c \sim T^{1/2}$, reflecting that this system behaves better as a set of Stoner–Wohlfarth particles. It was also found that there exists a critical thickness (~133 nm) for the 450 °C annealed (for 1 h) Fe–C ($x_v = 58$) granular films with thickness in the range 100–200 nm, below and above which the magnetization reversal is dominated by domain wall motion and by Stoner–Wohlfarth rotation, respectively.

[3] Author to whom any correspondence should be addressed.

1. Introduction

Nanocomposite films, consisting of nanoscale ferromagnetic metal particles, such as Fe, Co, Ni or their alloys, embedded in a host matrix, for example Cu, Ag, C, SiO_2, Al_2O_3, AlN, BN, etc, exhibit many interesting properties, such as enhanced coercivity, superparamagnetism, giant magnetoresistance or tunnelling magnetoresistance originating from finite-size and interface effects [1], and have many possibilities for use in various technological applications, such as high-density magnetic recording [2, 3]. Generally, magnetic metal particles are immiscible with a non-magnetic matrix, unless prepared by rapid quenching techniques, such as sputtering. The interactions between magnetic particles affect the coercivity of magnetic granular films greatly. However, optimum ferromagnetic metal composition, a suitable host matrix and complete phase segregation between magnetic particles and the non-magnetic matrix can reduce the interaction between magnetic granules. In this case, the volume fraction of the magnetic component is generally below the percolation threshold, and the well isolated magnetic particles are small enough to become magnetically single domain structures, in which the magnetic moment only rotates during the magnetizing procedure, causing high coercivity. Complete phase segregation between the particles and the matrix can be achieved by fabricating magnetic granular films at elevated substrate temperature and subsequent annealing at higher temperatures. One of the suitable host matrix materials is C because it can provide good magnetic isolation between neighbouring particles and reduce the interparticle exchange coupling [4]. Another important feature of C is that it can also protect the core material against outside degradation such as corrosion and attack by concentrated acids [5, 6]. Several groups have studied the structural and magnetic properties of Fe–C nanocomposite films prepared by different techniques, and revealed that the morphology and structure of ferromagnetic metal granular films are sensitive to preparation methods and conditions [7, 8]. In this paper, the Fe–C granular films were fabricated by a DC facing-target sputtering system at room temperature and subsequently annealed at different temperatures and time in 10^{-4} Pa vacuum. The annealing effects on the microstructures and magnetic properties were investigated in detail by using atomic force microscopy (AFM), x-ray photoelectron spectroscopy (XPS), x-ray diffraction (XRD), high-resolution transmission electron microscopy (TEM) and vibrating sample magnetometry (VSM).

2. Experimental details

The Fe–C ($45 \leqslant x_v \leqslant 85$) granular films with different Fe volume fraction x_v were fabricated by a DC facing-target sputtering system at room temperature. The distance between the two targets 100 mm in diameter was 100 mm. The base pressure of the chamber was better than 2.0×10^{-4} Pa and sputtering was carried out in a 0.5 Pa Ar (99.999%) atmosphere. One of the two targets was pure graphite (99.999%), and the other was pure Fe (99.999%) on which a piece of pure graphite (99.999%) was placed. The composition was controlled by changing the diameter of the C piece. The sputtering power was 190 W and the deposition rate was $\sim$0.3 Å s^{-1}. The thickness of the Fe–C films with different Fe volume fraction x_v was set at about 100 nm, except for Fe–C ($x_v = 58$) granular films whose thickness ranges from 100 to 200 nm. Cleaved NaCl, Si(100) wafers and microscope glass cover slips were used as substrates. All of the as-deposited Fe–C granular films were subsequently annealed at 450 °C for 1 h in a 10^{-4} Pa vacuum. Some of the as-deposited 100 nm thick Fe–C ($x_v = 58$) granular films on Si(100) wafer were annealed at temperatures ranging from 350 to 550 °C for 1 h, and at 450 °C for 30, 60, 90 and 120 min.

For planar-view TEM observation, we used free-standing Fe–C films, which were deposited on cleaved NaCl substrates and subsequently floated on distilled water to dissolve the

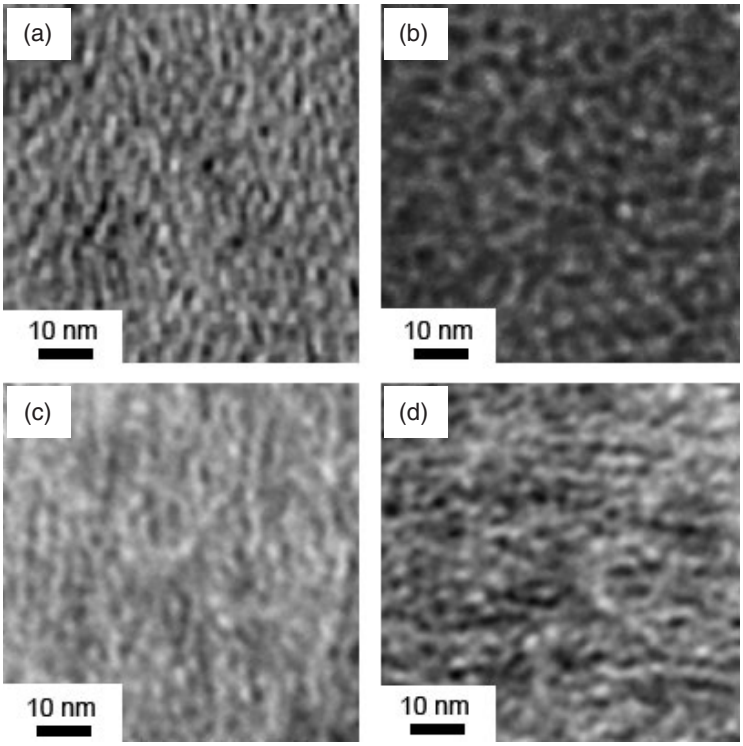

Figure 1. Planar-view bright field TEM images of 100 nm thick as-deposited Fe–C granular films with different Fe volume fractions: (a) $x_v = 49$, (b) $x_v = 58$, (c) $x_v = 65$ and (d) $x_v = 84$.

NaCl substrates. The composition of these granular films was analysed by XPS using Mg Kα radiation (1253.6 eV) with a resolution of about 0.25 eV. In order to remove the contaminated surface layer, Ar ions with 2 keV energy, a current density of 1 mA mm^{-2} and an incident angle of 45° were used to sputter the samples. The microstructure of the samples was analysed by XRD and selected area electron diffraction (SAED). The thickness of the films was measured by a Dektak profiler and also by calibrating the deposition rate. The magnetic properties were measured by a VSM at different temperatures and angles.

3. Results and discussion

3.1. Morphology and structure

Figure 1 gives the planar-view bright field TEM images of 100 nm thick as-deposited Fe–C granular films with different Fe volume fraction x_v. All the as-deposited Fe–C granular films are composed of ∼2–6 nm Fe granules embedded in a C matrix, which is the typical morphology of granular films. The granules are not regular but elliptical, and the size distribution is large when the Fe volume fraction is 49. At $x_v = 84$, Fe granules connect with each other because the Fe volume fraction is far above the percolation threshold (about 0.5–0.55). It is also clear that the Fe–C ($x_v = 58$) sample possesses relatively good granular structure with uniform grain size, as shown in figure 1(b), although some of the granules touch.

Figure 2 shows AFM micrographs of as-deposited and annealed Fe–C ($x_v = 58$) granular films deposited on Si(100). The surface roughness R_a is defined as the arithmetic average

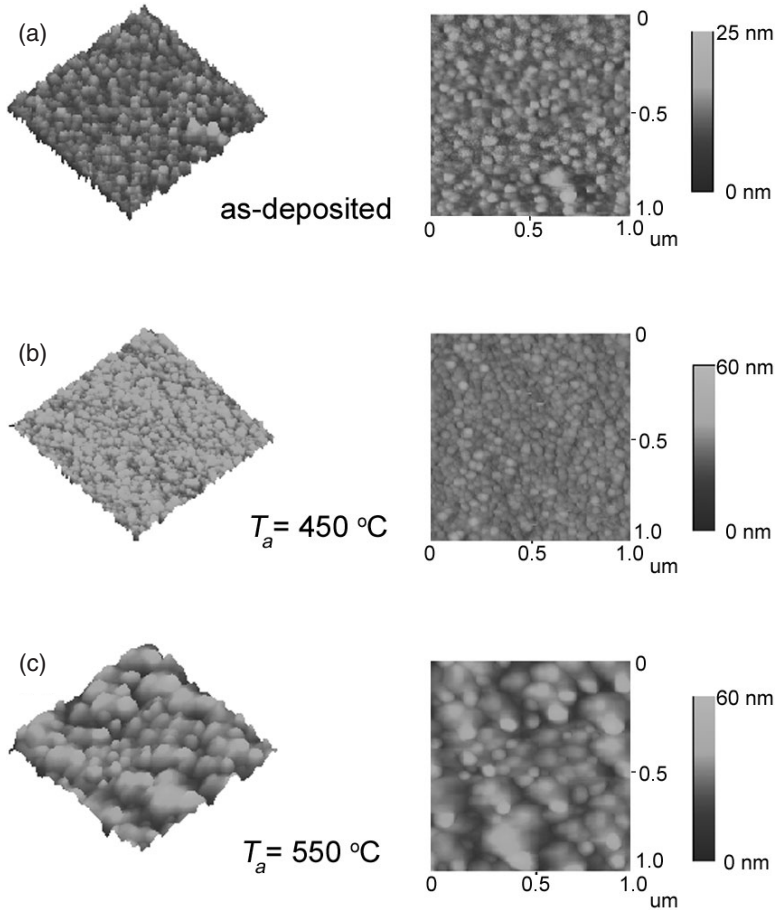

Figure 2. AFM micrographs of Fe–C ($x_v = 58$) granular films deposited on Si(100): (a) as-deposited, (b) annealed at 450 °C for 1 h and (c) annealed at 550 °C for 1 h.

deviation from the mean line within the assessment length L_a

$$R_a = \frac{1}{L}\int_{x=0}^{x=L_a} |y|\,dx, \tag{1}$$

where x is the displacement along the lateral scan direction and y is the vertical fluctuation. One can see from the figure that when annealing temperature increases, the average surface roughness of Fe–C ($x_v = 58$) granular films increases due to phase segregation, crystallization and increasing grain size. However, due to the aggregation of smaller particles, the R_a value of the samples annealed at 550 °C is smaller than that of the samples annealed at 500 °C, as shown in table 1, where we list the R_a values of the as-deposited and annealed samples.

Figure 3 presents the XRD patterns of as-deposited and annealed Fe–C ($x_v = 58$) granular films deposited on Si(100), indicating that the as-deposited and 350 °C annealed samples are composed of amorphous Fe and C, and the amorphous Fe crystallizes to α-Fe at higher annealing temperatures. At higher annealing temperatures of 500 and 550 °C, the relative intensity of α-Fe(110) increases, signalling a better crystallization at higher anneal temperatures. XPS measurements were performed with an emphasis on the peaks associated with Fe_{2p}, C_{1s} and O_{1s}. The intensity of the C_{1s} peak almost keeps constant after 3 min Ar^+

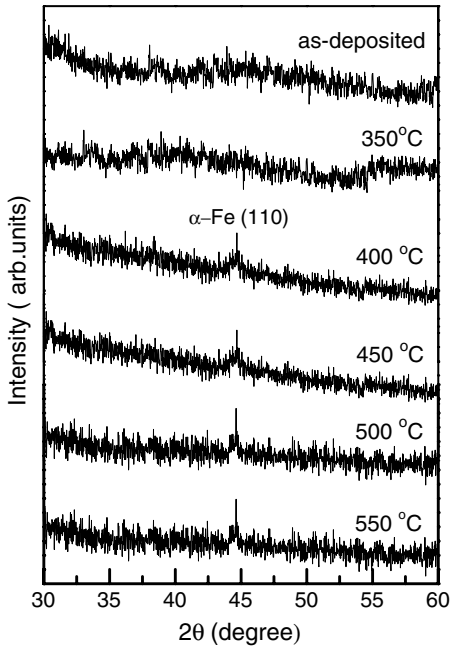

Figure 3. XRD patterns of as-deposited and different temperature 1 h annealed Fe–C ($x_v = 58$) granular films deposited on Si(100).

Table 1. The values of average roughness determined by AFM at different annealing temperatures.

Annealing temperature (°C)	Average roughness (nm)
As-deposited	1.433
350	1.583
400	1.693
450	1.988
500	6.249
550	5.140

ion bombardment (2 keV), indicating that the surface contaminated C has been cleaned off. Moreover, after 5 min of Ar^+ ion bombardment, the contaminated oxygen peaks also disappear. As shown in figure 4, the peaks situated at 284.6 and 707.5 eV in the C_{1s} and Fe_{2p} XPS spectra of as-deposited Fe–C ($x_v = 58$) granular films are from pure C and metallic Fe, respectively. The shoulders located at 710.3 and 723.4 eV, at the high energy side of Fe $2p_{3/2}$ and $2p_{1/2}$ peaks, corresponds to the Fe^{2+} ions from FeO [9], which can be due to the small amount of O_2 remaining in the chamber and/or that mixed in the Ar gas (99.999%). In addition, no iron carbide peaks (Fe_{2p} 708.5 eV) are visible, suggesting that no carbides are formed during the deposition, although Fe mixes with C in the incomplete phase-separating films.

Figure 5 shows the planar-view bright field TEM images and corresponding SAED patterns of 100 nm thick Fe–C ($x_v = 58$) granular films annealed at 450 and 550 °C for 1 h, and those of as-deposited samples are also presented for comparison. It is seen from figure 5(a) that the as-deposited film is composed of ∼4 nm Fe grains separated by the C matrix, and the Fe granules irregularly connect with each other because the Fe volume fraction in the films is near the percolation threshold. There are no sharp diffraction rings visible in the SAED

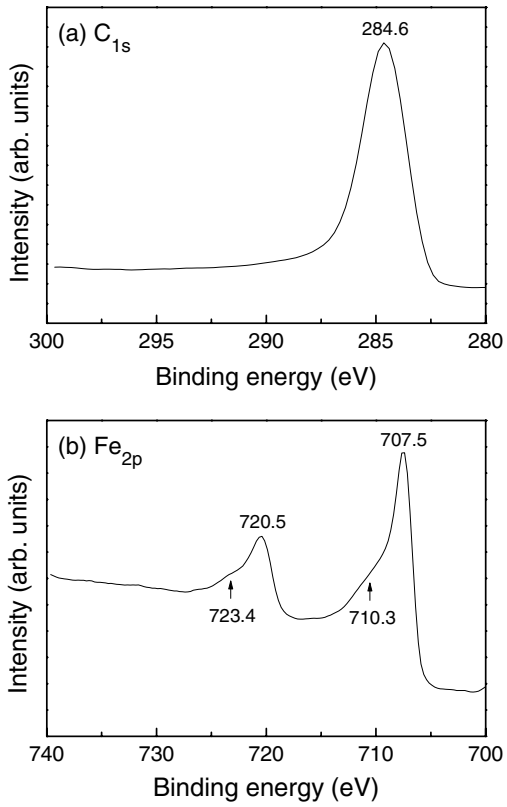

Figure 4. (a) C_{1s} and (b) Fe_{2p} XPS spectra for as-deposited Fe–C ($x_v = 58$) granular films.

pattern (figure 5(a)), reflecting that both Fe and C are amorphous in the as-deposited samples, because the substrate temperature is too low for Fe and C to crystallize during the deposition. This is consistent with the XRD result presented in figure 3. In figure 6, we show the high-resolution TEM image of 100 nm thick as-deposited Fe–C ($x_v = 58$) granular films, where the dark region corresponds to Fe particles and the bright area to C because of the different densities of amorphous Fe and C. It is thus clear that Fe and C phases have already separated during the film growth, although the segregation is not complete, just as in the case of Co–C granular films [10]. When the annealing temperature increases to 450 °C, the granules grow to ∼12 nm (figure 5(b)) and the SAED pattern corresponds to polycrystalline α-Fe. The phase segregation is more complete, and the Fe granules are embedded in the amorphous C matrix. Annealed at 550 °C, the granules grow to ∼50–100 nm, and the C phase has transformed from amorphous C to graphite-like C, which can be ascribed to the catalysis of Fe particles on the graphitization [11], as shown in figure 5(c). Figure 7 displays the high-resolution TEM images of Fe lattice fringes. The spacing of the particle shown in figure 7 is ∼0.2 nm, which is nearly equal to that of bcc Fe(110) (0.21 nm), indicating that high temperature annealing significantly improves the crystallinity of Fe granules. The inset in figure 7 is the fast Fourier transform (FFT) image of the Fe lattice, obtained by using DigitalMicrograph software. Similar to SAED, FFT presents the diffraction pattern of a lattice in reciprocal space. There exists only a pair of dots and no other dots appear, indicating that only one set of lattices exists in figure 7, and further confirming the existence of the pure bcc Fe(110) phase (also see figure 5(c)).

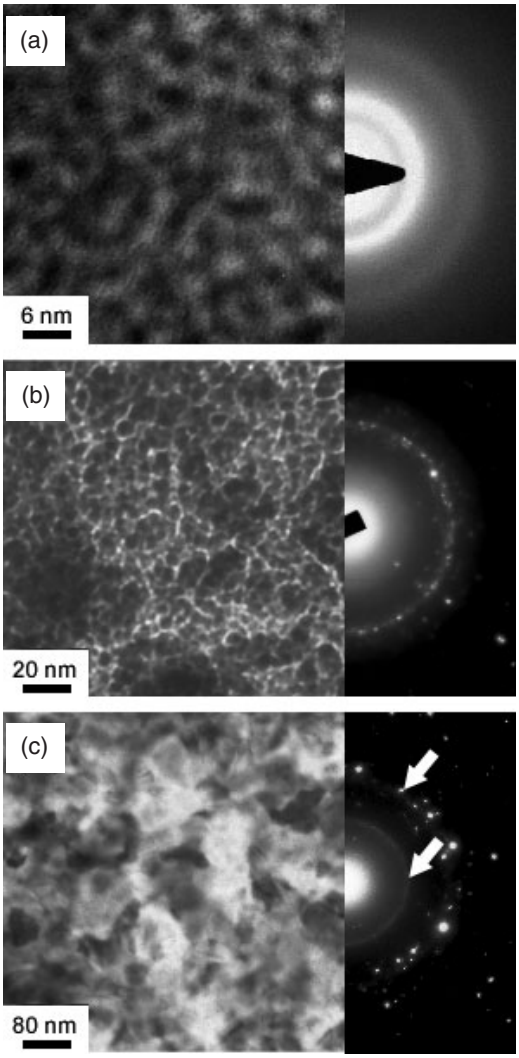

Figure 5. Planar-view bright field TEM images of 100 nm thick Fe–C ($x_v = 58$) granular films, (a) as-deposited, (b) annealed at 450 °C, (c) annealed at 550 °C, and corresponding SAED patterns. The inner ring is identified as graphite (002) and the outer ring as Fe bcc (110) in figure 5(c).

3.2. Magnetic properties

Figure 8 presents the in-plane M–H curves of 100 nm thick as-deposited Fe–C ($x_v = 58$) granular films measured at room temperature and 80 K, showing that the samples are superparamagnetic at room temperature and soft ferromagnetic at 80 K, which indicate that the interactions between ∼4 nm Fe granules exist in the 100 nm thick as-deposited Fe–C ($x_v = 58$) granular films, and the interactions may include the dipolar interaction between the magnetic particles (direct) and exchange coupling through the Fe atoms buried in the C matrix (indirect) due to the incomplete phase segregation between Fe and C phases (see figure 6). However, these interactions are not enough to avoid superparamagnetism at room temperature. Under the assumption of weak magnetic interaction between particles, the M–H curve measured at

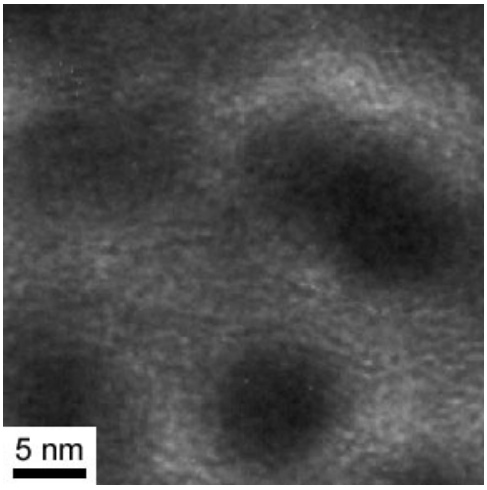

Figure 6. High-resolution TEM image of 100 nm thick as-deposited Fe–C ($x_v = 58$) granular films.

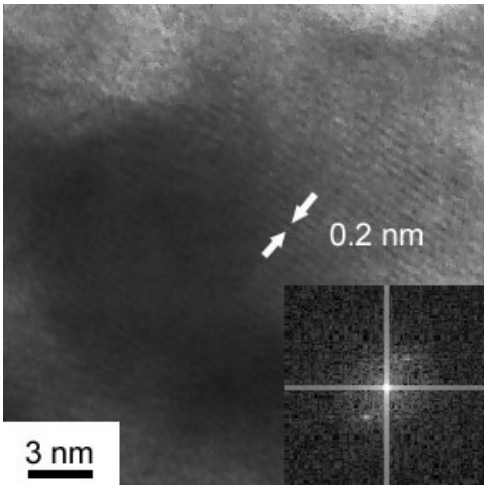

Figure 7. High-resolution TEM, and corresponding fast Fourier transform, image of Fe–C ($x_v = 58$) granular films annealed at 550 °C.

room temperature can be described by a Langevin function [12]

$$M(H) = M_s\left(\coth\left(\frac{\mu H}{k_B T}\right) - \frac{k_B T}{\mu H}\right), \tag{2}$$

where μ ($=M_s V$) is the magnetic moment of a single particle with volume V, M_s saturation magnetization and k_B Boltzmann constant. Considering the size distribution in real systems, the resultant magnetization should be given by

$$M(H) = M_s \int_0^\infty L\left(\frac{M_s V H}{k_B T}\right) f(V)\,\mathrm{d}V, \tag{3}$$

where L is the Langevin function and $f(V)$ the size distribution. Assuming spherical particles

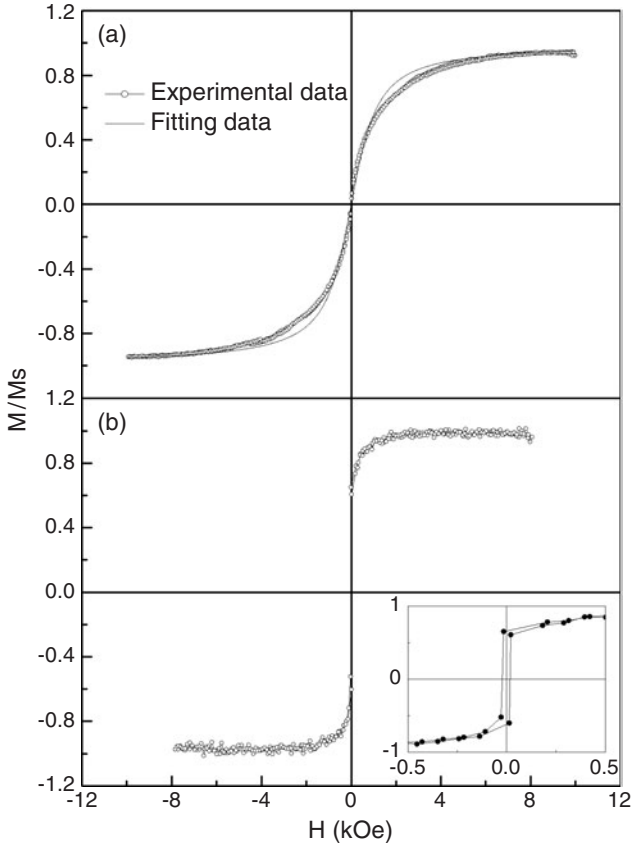

Figure 8. In-plane magnetization curve of as-deposited Fe–C ($x_v = 58$) granular films measured at (a) room temperature and (b) 80 K.

of diameter D for simplicity, a log-normal size distribution

$$f(D) = \frac{1}{\sqrt{2\pi}\ln\sigma D}\exp\left[-\frac{\left(\ln D - \ln \overline{D}\right)^2}{2(\ln\sigma)^2}\right], \tag{4}$$

with

$$\int_0^\infty f(D)\,\mathrm{d}D = 1, \tag{5}$$

is most often used. The grain size obtained by fitting the magnetization curve of as-deposited Fe–C ($x_v = 58$) granular films is ~4.5 nm and the value of $\ln\sigma$ is ~0.3. The former is consistent with the granule size estimated from the high-resolution TEM image shown in figure 6.

Figure 9 presents the in-plane and out-of-plane room-temperature M–H curves of the 100 nm thick Fe–C ($x_v = 58$) granular films annealed at 450 and 550 °C for 1 h, indicating that the easy axis is in the film plane. The saturation magnetization of the annealed 100 nm thick Fe–C ($x_v = 58$) granular films almost does not change with the annealing temperature ranging from 350 to 550 °C (for 1 h) and annealing time (at 450 °C). Figure 10 shows the in-plane room-temperature coercivity versus annealing temperature and time for the annealed Fe–C ($x_v = 58$) granular films. The in-plane coercivity measured at room temperature increases

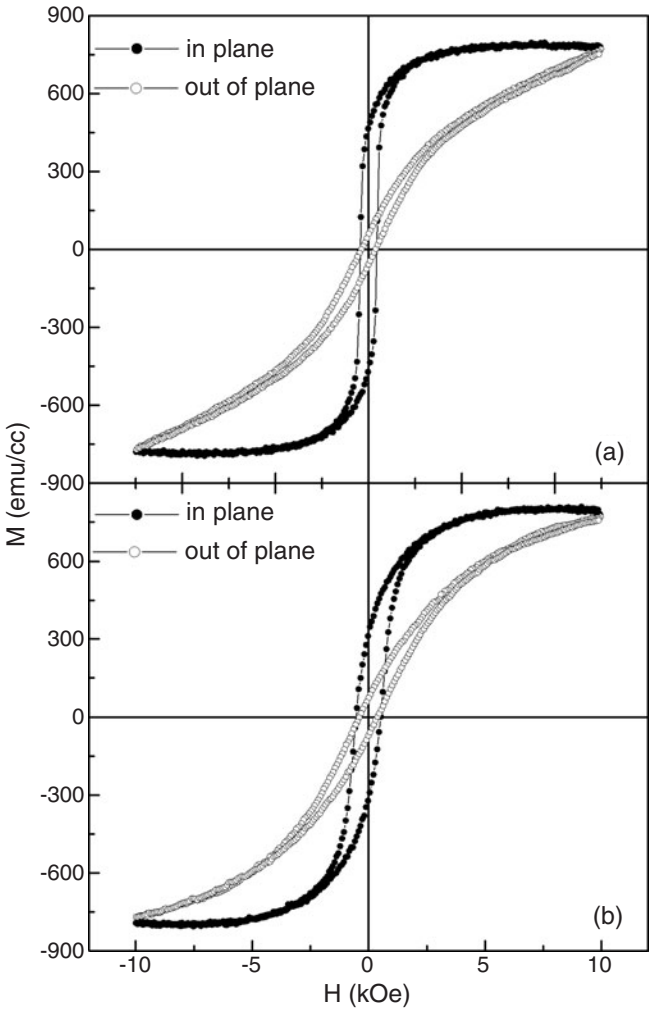

Figure 9. In-plane and out-of-plane magnetization curves measured at room temperature of 100 nm thick Fe–C ($x_v = 58$) granular films annealed at (a) 450 and (b) 550 °C.

with the increase of annealing temperature and time. For films annealed at 400 °C, the in-plane coercivity is ∼200 Oe. The following reasons may be responsible for the relatively small coercivity:

(1) the magnetic interactions, including dipolar interaction between ferromagnetic particles and exchange coupling between granules via the Fe atoms dispersed in the C matrix, are strong because the phase segregation is not complete, and
(2) the size of granules is smaller than that of granules annealed at higher temperatures.

In the literature, observation of long-range domain structures caused by exchange interactions through the metallic matrix in heterogeneous granular alloys and by dipolar interactions in ferromagnetic nanocomposites has been reported [13–18]. Therefore, the increase of coercivity with annealing temperature and time are possibly in part due to the suppression of the formation of long-range domain structures caused by phase segregation and increase in granule size.

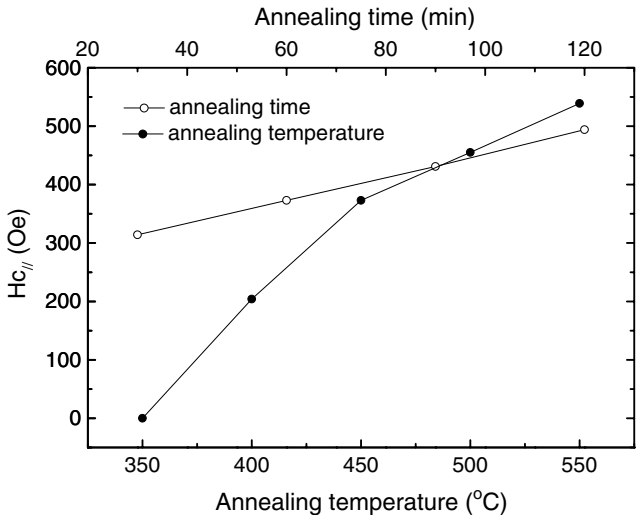

Figure 10. In-plane room-temperature coercivity as a function of annealing temperature (for 1 h) and time (at 450 °C), for the 100 nm thick Fe–C ($x_v = 58$) granular films.

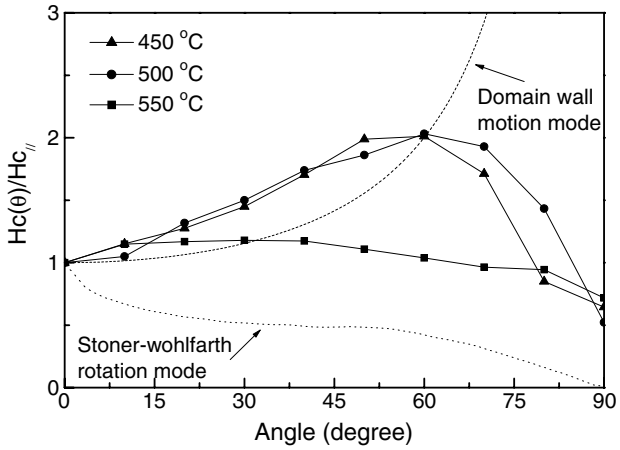

Figure 11. Angular dependence of room-temperature coercivity for Fe–C ($x_v = 58$) granular films annealed at different temperatures.

Figure 11 presents the angular dependence of room-temperature coercivity for Fe–C ($x_v = 58$) granular films annealed at different temperatures. Also shown in the figure are the $H_c(\theta)/H_{c\|}$ versus θ curves calculated based on the domain wall motion mode and the Stoner–Wohlfarth rotation mode. The ideal domain wall motion mode should follow the $H_c(\theta) \sim 1/\cos\theta$ relation, where θ is the angle between the applied field and the film plane [19]. It is suggested from the figure that the magnetization reversal mechanism changes with annealing temperature. Below 500 °C, the magnetic reversal mechanism approximately obeys the ideal domain wall motion mode at angles smaller than 60°, which can be ascribed to the fact that the granules are not completely independent of each other (see figure 5) and some magnetic interactions still exist between particles at low annealing temperatures. But at the angles above 60°, the mechanism deviates from the ideal domain wall motion

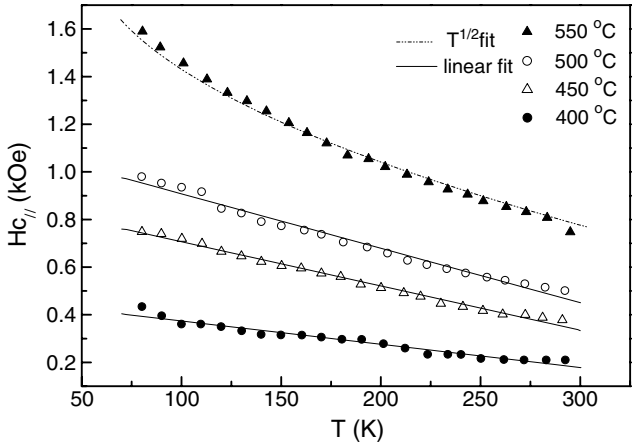

Figure 12. In-plane coercivity versus measuring temperature for Fe–C ($x_v = 58$) granular films annealed at different temperatures for 1 h.

significantly. Thus the reversal mechanism seems to involve not only domain wall motion but also a rotational mode. At 550 °C, the magnetization reversal can be well described by the Stoner–Wohlfarth rotation mode over the whole angle range. This change in the magnetization reversal mechanism is due to the complete segregation of granules during higher temperature annealing, whose reversal mechanism has been proved experimentally to follow the Stoner–Wohlfarth rotation mode [20]. However, the out of plane coercivity of all annealed samples is not zero (see figures 9 and 11), which does not critically follow the Stoner–Wohlfarth rotation mode with zero out-of-plane coercivity. This discrepancy may be due to the magnetostatic interaction between magnetic particles that prevents the particle rotating at higher angles [21].

In order to further investigate the magnetization reversal mechanism, the temperature dependence of H_c has been measured. Figure 12 shows the dependence of in-plane coercivity on the measuring temperature of Fe–C ($x_v = 58$) granular films annealed at different temperatures for 1 h. The in-plane coercivity decreases monotonically with the increase of measuring temperature, dropping from 1590 Oe at 80 K to 719.5 Oe at 295 K for a sample annealed at 550 °C, 980.4 to 501 Oe for 500 °C, 748.5 to 378.3 Oe for 450 °C and 434 to 210 Oe for 400 °C. This decrease in coercivity with temperature can be interpreted as the contribution of intrinsic temperature dependence of the anisotropy and magnetization, and thermal activation effects [17]. Assuming that the film consists of independent, aligned Stoner–Wohlfarth particles, $H_c(T)$ can thus be given by [22, 23]

$$H_c(T) = \eta H_K \left[1 - \left(\frac{25 k_B T}{K_u V} \right)^{1/2} \right], \tag{6}$$

where $\eta = 1$, $K_u = M_s H_K/2$ and V is the particle volume. For the sample annealed at 550 °C, the tendency of the change of in-plane coercivity with T satisfies the relation $H_c \sim T^{1/2}$ (equation (5)), reflecting that the system behaves as a set of Stoner–Wohlfarth particles. Bean and Livingstone suggested that the relation between coercivity and temperature satisfied the characteristic $T^{1/2}$ law for systems composed of monodisperse aligned particles without magnetic interactions [23, 24]. However, Pfeiffer *et al* reported that for an assembly of randomly oriented particles, H_c could be plotted against $T^{0.77}$ [25]. In our case, the maximum magnetic field was applied prior to measuring the coercivity so that the particles were aligned. Therefore, the particles should follow the $T^{1/2}$ law. But the coercivity of samples annealed

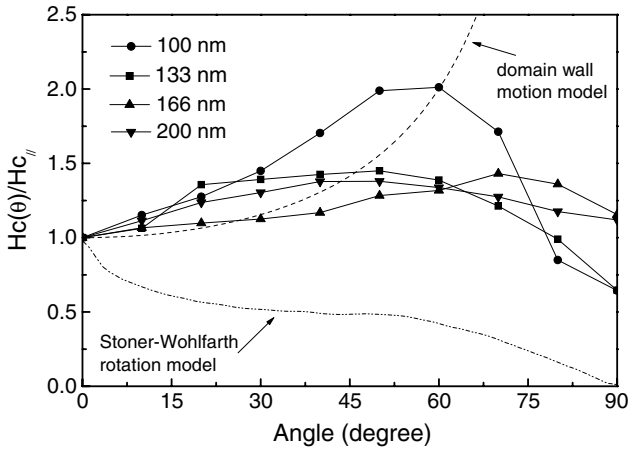

Figure 13. Angular dependence of room-temperature coercivity for 450 °C annealed Fe–C ($x_v = 58$) granular films with different film thicknesses.

at 400, 450 and 500 °C decreases linearly with the increase of temperature, signalling that these systems are not composed of Stoner–Wohlfarth particles and a new mechanism should be introduced to explain this behaviour. Gaunt [26] suggested that the coercivity caused by domain wall pinning can be expressed as

$$H_c(T) = H_0\left[1 - \left(\frac{25k_BT}{E_0}\right)^{\beta}\right], \tag{7}$$

where H_0 is the coercivity at zero temperature, representing the intrinsic coercivity of materials, and E_0 the domain wall energy. Obviously, the relations between in-plane coercivity and temperature shown in figure 12 for the Fe–C ($x_v = 58$) granular films annealed at 400, 450 and 500 °C can be well described by equation (7), and each corresponds to $\beta = 1$ [19, 26]. These indicate that the domain wall motion is the dominant mechanism for the coercivity.

Finally, the angular dependence of room-temperature coercivity for the 450 °C annealed Fe–C ($x_v = 58$) granular films with different film thicknesses is given in figure 13. It indicates that when the film thickness $t < 133$ nm, the magnetization reversal mechanism is mainly domain wall motion, but at $t \geqslant 133$ nm, the magnetization reversal mechanism is dominated by Stoner–Wohlfarth rotation, which can be explained by the structural constriction of the formation of single Fe granules at smaller film thickness [27]. The shape and size of the Fe granules, the number of neighbouring particles and the percolation threshold of samples are constricted by the film dimensions [14, 27, 28]. For example, under the constriction of film thickness, the particles cannot grow larger and the magnetic properties of the film will be greatly affected.

4. Conclusions

The structure, morphology and magnetic properties of as-deposited and annealed Fe–C granular films sputtered by a DC facing-target sputtering system at room temperature were studied. XRD, TEM and SAED show that the as-deposited and low-temperature annealed ($\leqslant$350 °C) Fe–C ($x_v = 58$) granular films are composed of amorphous Fe and C, and the amorphous Fe is crystallized to α-Fe by higher temperature annealing, which are confirmed by HRTEM

analyses. Magnetic measurements indicate that at room temperature the 100 nm thick as-deposited Fe–C ($x_v = 58$) granular films are superparamagnetic and annealed samples are ferromagnetic. The coercivity of the 100 nm thick annealed Fe–C ($x_v = 58$) granular films increases with annealing temperature (for 1 h) and time (at 450 °C). The magnetization reversal behaves as domain wall motion at annealing temperatures below 500 °C and as Stoner–Wohlfarth rotation when the annealing temperature increases to 550 °C, which is also evidenced by the changes in in-plane coercivity with measuring temperature. The film thickness dependence of in-plane coercivity shows that there exists a critical thickness, below which the magnetization reversal is dominated by domain wall motion and above by Stoner–Wohlfarth rotation.

Acknowledgments

The work described in this paper is supported by the National Science Foundation of China (50172033 and 50371061). The authors are grateful to Dr D F Kuang for AFM observations.

References

[1] Batlle X and Labarta A 2002 *J. Phys. D: Appl. Phys.* **35** R15
[2] Xiao J Q, Jiang J S and Chien C L 1992 *Phys. Rev. Lett.* **68** 3749
[3] Berkowitz A E, Mitchell J R, Carey M J, Young A P, Zhang S, Spada F E, Parker F T, Hutten A and Thomas G 1992 *Phys. Rev. Lett.* **68** 3745
[4] Host J J, Block J A, Parvin K, Dravid V P, Alpers J L, Sezen T and Laduca R 1998 *J. Appl. Phys.* **83** 793
[5] Ruoff R S, Lorents D C, Chan B, Malhotra R and Subramoney S 1993 *Science* **259** 346
[6] Jiao J and Seraphin S 1998 *J. Appl. Phys.* **83** 2442
[7] Babonneau D, Briatico J, Petroff F and Naudon A 2000 *J. Appl. Phys.* **87** 3432
[8] Hayashi T, Hirono S, Tomita M and Umemura S 1996 *Nature* **381** 772
[9] Bonnet F, Ropital F, Lecour P, Espinat D, Huiban Y, Gengembre L, Berthier Y and Marcus P 2002 *Surf. Interface Anal.* **34** 418
[10] Mi W B, Guo L, Jiang E Y, Li Z Q, Wu P and Bai H L 2003 *J. Phys. D: Appl. Phys.* **36** 2393
[11] Agostino R G, Caruso T, Chiarello G, Cupolillo A, Pacile D, Filosa R, Formoso V, Colavita E and Papagno L 2003 *Phys. Rev.* B **68** 045413
[12] Chien C L 1991 *J. Appl. Phys.* **69** 5267
[13] Franco V, Batlle X and Labarta A 2000 *Eur. Phys. J.* B **17** 43
[14] Sahimi M 1994 *Applications of Percolation Theory* (London: Taylor and Francis) chapter 12, and references therein
[15] Gavrin A, Kelley M H, Xiao J Q and Chien C L 1995 *Appl. Phys. Lett.* **66** 1683
[16] Batlle X, Franco V, Labarta A, Watson M L and O'Grady K 1997 *Appl. Phys. Lett.* **70** 132
[17] Kleemann W, Petracic O, Binek Ch, Kakazei G N, Pogorelov Yu G, Sousa J B, Cardoso S and Freitas P P 2001 *Phys. Rev.* B **63** 134423
[18] Sankar S, Berkowitz A E and Smith D J 2000 *Phys. Rev.* B **62** 14273
[19] Sangki J, Hsu Y N, Laughlin D E and McHenry M E 2000 *IEEE Trans. Magn.* **36** 2336
[20] Chikazumi S 1997 *Physics of Ferromagnetism* (Oxford: Clarendon) p 495
[21] Zhang L and Manthiram A 1996 *Phys. Rev.* B **54** 3462
[22] Sellmyer D J, Luo C P, Yan M L and Liu Y 2001 *IEEE Trans. Magn.* **37** 1286
[23] Bean C P and Livingstone J D 1959 *J. Appl. Phys.* **30** 120S
[24] Batlle X, Garcfa M M, Tejada J, Pfeiffer H, Gornert P and Sinn E 1993 *J. Appl. Phys.* **74** 3333
[25] Pfeiffer H and Schuppel W 1990 *Phys. Status Solidi* a **119** 259
Pfeiffer H 1990 *Phys. Status Solidi* a **120** 233
[26] Gaunt P 1983 *Phil. Mag.* B **48** 261
[27] Yu M, Liu Y and Sellmyer D J 1999 *J. Appl. Phys.* **85** 4319
[28] Butera A, Klemmer T J and Barnard J A 1998 *J. Appl. Phys.* **83** 4855